Available online at www.sciencedirect.com

ScienceDirect

Geochimica et Cosmochimica Acta 170 (2015) 39–50

Geochimica et Cosmochimica Acta

www.elsevier.com/locate/gca

The confines of triple oxygen isotope exponents in elemental and complex mass-dependent processes

Huiming Bao [a,b,*], Xiaobin Cao [a], Justin A. Hayles [a]

[a] Department of Geology & Geophysics, Louisiana State University, USA

[b] State Key Laboratory of Ore Deposit Geochemistry, Institute of Geochemistry, Chinese Academy of Sciences, Guiyang 550002, China

Received 17 September 2014; accepted in revised form 28 July 2015; available online 22 August 2015

Abstract

Small differences in triple isotope relationships, or $\Delta^{17}O$ in the case of oxygen, have been increasingly used to study a range of problems including hydrological cycles, stratosphere-troposphere exchange, biogeochemical pathways and fluxes, and the Moon's origin in the geochemical and cosmochemical communities. A $\Delta^{17}O$ value depends on the triple isotope exponent θ of involved reaction steps. However, the probabilistic distribution of the intrinsic and apparent θ values has not been examined for elemental processes and for processes that are out of equilibrium or bearing reservoir-transport complexities. A lack of knowledge on the confines of θ may hamper our understanding of the subtle differences among mass-dependent processes and may result in mischaracterization of a set of mass-dependent processes as being in violation of mass-dependent rules. Here we advocate a reductionist approach and explore θ confines starting from kinetic isotope effects (*KIE*s) within the framework of transition state theory (TST). The advantage of our *KIE* approach is that any elemental or composite, equilibrium or non-equilibrium process can be reduced to a set of *KIE*s with corresponding θ_{KIE}.

We establish that the *KIE* between a reactant and a transition state (TS) is intrinsic. Given a range of *KIE*s known for Earth processes involving oxygen, we use a Monte Carlo calculation method and a range of oxygen-bonded molecular masses to obtain a distribution of θ_{KIE} values and subsequently that of θ_{eq}. Next, complexities are examined by looking into expected effects due to reaction progress, unbalanced fluxes, and reference frame. Finally, compounded reservoir-transport effects are examined using two simple processes – Rayleigh Distillation (RD) and Fractional Distillation (FD). Our results show that the apparent θ values between two species or two states of the same evolving species have much broader confines than the commonly used "canonical" confines of 0.51–0.53, particularly when the overall fractionation factors are close to 1.000. Equilibrium processes exhibit the narrowest α-θ value distribution. More complex processes or non-equilibrium further broaden the confines of the apparent θ values for reaction systems. The compounded reservoir-transport effects of RD and FD demonstrate that non-canonical apparent θ and large non-zero $\Delta^{17}O$ values are achievable even when all involved elemental steps are strictly mass-dependent. This study calls for a research effort to determine *KIE* and θ_{KIE} for important natural processes, and for cautions in interpreting a slope value drawn in a $\delta'^{17}O$–$\delta'^{18}O$ space, as the slope is only a superficial manifestation of a set of complex reaction pathways and dynamics.

1. INTRODUCTION

In a physical, chemical, or biological process, oxygen-bearing species go through a re-distribution of $^{18}O/^{16}O$ as well as $^{17}O/^{16}O$ ratios, which are expressed correspondingly as isotope fractionation factors α^{18} and

* Corresponding author at: Department of Geology & Geophysics, Louisiana State University, USA. Tel.: +1 225 5783419.
E-mail address: bao@lsu.edu (H. Bao).

http://dx.doi.org/10.1016/j.gca.2015.07.038
0016-7037/

α^{17} ($\alpha \equiv R_A/R_B$; $R = {}^{18}O/{}^{16}O$ or ${}^{17}O/{}^{16}O$; and A and B can be two species or the same species at two different times). At high temperatures, the logarithm of the equilibrium isotope effect $ln\alpha$ is proportional to the product of $F * \Delta m/(m_1 * m_2)$, in which F is the force constant of O bond and m_1 and m_2 are two of the oxygen isotopes, say, ^{16}O and ^{18}O, or ^{16}O and ^{17}O (Bigeleisen, 1949, 1965). Because F is the same for isotopologues, the ratio of $ln\alpha^{17}/ln\alpha^{18}$ is then related simply to isotope masses. If we denote θ for this ratio, θ assumes a value of 0.5305 for the triple oxygen isotope system.

The θ values for equilibrium processes at −50 °C to 1000 °C have been explored theoretically by Cao and Liu (2011), in which an equilibrium θ between any oxygen-bearing species A and B is obtained by calculating α_A, β_A, α_B, and β_B using quantum chemistry methods based on the Bigeleisen–Mayer equation. The introduction of a new concept κ, defined as $ln\beta^{17}/ln\beta^{18}$, which is the equilibrium θ value for an isotope exchange reaction between an O-bearing species and the ideal gaseous monatomic O, simplified the θ_{eq} calculation. It is found that at temperatures from −50 °C to 1000 °C, κ has a rather narrow range varying from 0.5275 to 0.5303 for all β or reduced partition function ratios (*RPFRs*). Here the lower value 0.5275 is calculated based on one of the strongest bound oxygen species CO_2. Given the corresponding κs, the θ was then found to vary from 0.523 to 0.526 for examined mineral–water equilibrium exchange cases, with an approx. 0.001 increase per 100 °C temperature increase. The apparent narrow θ range is based on a few pairs and is not the general picture. The full confines of the θ_{eq} need to be explored.

An overall restricted range of θ_{eq} would produce a tight linear correlation between $\delta'^{18}O$ and $\delta'^{17}O$, defined as $ln(R_{sample}/R_{reference})$, among oxygen-bearing species on Earth, which is indeed manifested as the terrestrial fractionation line (Clayton et al., 1973; Rumble et al., 2007). Recently, thanks to the increasing resolving power of analytical tools, smaller and smaller differences in the relationship between $\delta'^{18}O$ and $\delta'^{17}O$, or $\Delta^{17}O$ differences ($\Delta^{17}O \equiv \delta'^{17}O - C \times \delta'^{18}O$, and C is an assigned straight-line slope value in a $\delta'^{18}O$–$\delta'^{17}O$ space), have been measured and interpreted in geochemical literature. Small mass-dependent deviations in the ^{17}O content in water have become an added dimension to understanding the kinetics of hydrological cycles (Angert et al., 2004; Barkan and Luz, 2005, 2007; Luz and Barkan, 2005; Landais et al., 2006, 2012). Approx. 0.2‰ $\Delta^{17}O$ differences are also reported among seawater, sedimentary rocks, and mantle rocks (Levin et al., 2014; Pack and Herwartz, 2014; Passey et al., 2014; Herwartz et al., 2015). Small non-mass-dependent ^{17}O anomalies in modern atmospheric O_2 was recognized earlier (Luz et al., 1999) and applied to quantify biogeochemical cycling (Blunier et al., 2002; Angert et al., 2003; Hendricks et al., 2005), while questions remain on the exact magnitude of those ^{17}O anomalies (Young et al., 2002, 2014; Bao et al., 2008). The small ^{17}O anomalies in air O_2 have inspired an effort to explore its utility in animal physiology, diagenesis, and the geological O_2 record in phosphate minerals (Gehler et al., 2011; Pack et al., 2013). Small $\Delta^{17}O$ differences have also been predicted (Hoag et al., 2005) and reported (Thiemens et al., 2014) for tropospheric CO_2. The improved analytical capacity has resulted in a further survey of terrestrial (e.g. Rumble et al., 2007) and lunar (Herwartz et al., 2014) triple oxygen isotope compositions. Concepts and the underlying mechanisms for the observed small mass-dependent $\Delta^{17}O$ differences have been explored (Miller, 2002; Young et al., 2002). There are also phenomena displaying non-canonical triple oxygen or triple sulfur isotope relationships that should otherwise be purely mass-dependent. For example, SF_6 ice–vapor equilibrium at low T (137–173 K) has a $^{33}\theta$ value of ca. 0.55, significantly beyond the cononical value of ca. 0.52 (Eiler et al., 2013). A slow thermal decomposition of carbonate minerals by laser heating can generate CO_2 that is ca. 0.20‰ higher than the residue CaO in $\Delta^{17}O$ (Miller et al., 2002). A modeling study on microbial sulfate uptake also demonstrates that when the overall degree of sulfur isotope fractionation $\Delta\delta^{34}S$ is small, e.g. less than 15‰, the apparent $^{33}\theta$ would deviate from the equilibirum value of 0.515 and become as low as 0.508 (Wing and Halevy, 2014). In addition, Sun and Bao (2011a,b) reported up to 1‰ difference in $\Delta^{17}O$ between O_2 gases at the two temperature ends of a thermal gradient. The current rapidly increased geochemical literature on small $\Delta^{17}O$ and similarly on small $\Delta^{33}S$ is in need of a critical evaluation. While it is important to examine individual cases reported in literature, we first address a question that is at the very foundation of the $\Delta^{17}O$ value differences or deviations: What are the confines of θ for mass-dependent processes? Or can an apparent non-canonical θ value or a distinct non-zero $\Delta^{17}O$ value be expected for a process in which each of its elemental steps is strictly mass-dependent? In this study, a "canonical" θ value is loosely placed in the range of 0.51–0.53.

As illustrated above, the confines of θ are not fully known even for equilibrium processes, let alone for non-equilibrium processes in nature. Note that an equilibrium process refers to a process in which forward and backward reactions go through the same transition state (TS) with the same fluxes. Thus, non-equilibrium process refers to any process that does not have equal backward and forward fluxes or in which the backward and forward reactions link to different TSs. In that sense, steady-states with equal backward and forward reaction fluxes with respect to a species of interest but which link to different TSs are also non-equilibrium processes. To explore both equilibrium and non-equilibrium processes, we start from the transition state theory (TST) or the Absolute Rate Theory (Eyring, 1935). TST states that there is a barrier between a reactant and a product along its reaction coordinate, and the TS is on the top of the barrier and it is at quasi-equilibrium with the reactant (Eyring, 1935; Felipe et al., 2001). In other words, we shall derive the triple oxygen isotope relationships for equilibrium and non-equilibrium processes starting from the kinetic isotope effect (*KIE*), i.e. θ_{KIE} for the reactant-TS step.

Unfortunately, research efforts in calibrating *KIE* or θ_{KIE} for the many important natural processes is embarrassingly spare at this moment. Therefore, in this paper, we will first model the confines of θ_{KIE} for the fundamental

reactant-TS steps for typical physical and chemical processes on the Earth. Then, the confines of θ for equilibrium processes or θ_{eq}, the only other intrinsic θ, are examined. Once we have the two types of intrinsic θs, we explore the apparent αs and θs of typical non-equilibrium processes. Our treatment is not based on a specific case but on a statistical ground using the Monte Carlo method. The result offers us a probabilistic distribution of the apparent θ values for combinations of mass-dependent processes. Finally, the importance of compounded reservoir-transport effects on apparent θ and Δ values is illustrated using Rayleigh Distillation and Fractional Distillation process models. Our study conveys a reductionist conceptual framework from which observational θs and Δs can be properly interpreted. Evidently, the considered θ and Δ issues are not restricted to oxygen. Hydrogen (H, D, and T), carbon (12, 13, 14), and sulfur (32, 33, 34, 36), as well as many other systems have similar issues and debates (Bigeleisen and Wolfsberg, 1953; Stern and Vogel, 1971; Hirschi and Singleton, 2005; Sun and Bao, 2011a; Eiler et al., 2013). The conclusion drawn from this study can be applied to these other multiple isotope systems as well. In fact, our work was in part inspired by Hirschi and Singleton (2005) in which the three hydrogen isotope (HDT) relationship or the Swain-Schaad exponent is examined for secondary *KIE*s that have no tunneling or kinetic complexities.

2. MODELING STRATEGY, INDEPENDENT VS. DEPENDENT VARIABLES

To go from a fundamental reactant-TS step to complex processes in nature, we first examine the confines of θ_{KIE} for reactant-TS at a given range of *RPFR*s for $^{18}O/^{16}O$. Then we consider θ for an equilibrium case, θ_{eq}, when two reactant-TS steps share the same TS and have the same reaction rate of opposite signs. Confines of apparent θ in non-equilibrium processes are examined through reaction progress, unbalanced forward and backward fluxes, and reference frame. We only examine processes where analytical solutions are obtainable for the apparent θ of a process. Monte Carlo calculation is used to explore the confines of apparent θ as dictated by the analytical solutions.

It is important to point out that in our Monte Carlo calculation, mass and *RPFR* for $^{18}O/^{16}O$ are independent variables, whereas the corresponding *RPFR* for $^{17}O/^{16}O$ is not an independent variable. A $RPFR^{17}$ is constrained by its value being equal to $(RPFR^{18})^{\kappa}$, in which κ is the equilibrium θ value of an isotope exchange reaction between an O-bearing species and the ideal gaseous monatomic O. κ has a narrow range of 0.5275–0.5305 as pointed out above (Cao and Liu, 2011), thus providing a good constraint on the corresponding $RPFR^{17}$ as long as $RPFR^{18}$ is set in our Monte Carlo model. This is the only three oxygen isotope coupling being considered in this study. There may exist a loose link between the values of *RPFR* and κ for diatomic species, but we treat *RPFR* and κ as uniformly distributed and uncorrelated in this study. After the confines of θ_{KIE} are determined, subsequent modeling on equilibrium and non-equilibrium processes will use the confines of θ_{KIE} to constrain $RPFR^{17}$ at given model-input of $RPFR^{18}$.

Sets of 40–100 million uniformly distributed pseudo-random numbers bounded by their respective ranges are used as model inputs. The Mersenne-Twister algorithm is used to generate the random numbers as used by default in the program R (Matsumoto and Nishimura, 1998; R Development Core Team, 2012). The number of model runs is adjusted to between 40 and 100 million to compensate for the small bandwidth used for point density estimation and regions of sparse population in some models. Color plots are generated by a transformation of a binned kernel density estimate using a fixed bandwidth of 0.1% or less of the corresponding axis length (Wand, 2014). The transformation of the kernel density estimate used for plots consists of converting the 2-D kernel density estimate, to a 2-D probability mass function, sorting the probability mass function from highest to lowest value, and performing a cumulative sum for all values. The resulting cumulative sum value corresponds to an estimate of the probability of that location, and any location with a higher probability density, e.g. 25%, 50% and 75% (Wickham, 2009). When printed in gray scale, the center indicates higher density (probability) while the edges lower density (probability) (Monte Carlo calculation codes can be found in Supplementary data).

3. θ_{KIE}

3.1. Model parameters

Considering a typical chemical reaction,

$$A \leftrightarrow A^{\ddagger} \rightarrow B$$

where A is reactant, $A^{\ddagger}$ is transition state, and B is the product. From transition state theory, the reaction rate constant can be calculated by (Bigeleisen and Wolfsberg, 1958)

$$k = \frac{k_B T}{h} K^{\ddagger} \Gamma \tag{1}$$

where k_B is Boltzmann constant, T is temperature in Kelvin, h is Planck's constant, $K^{\ddagger}$ is the equilibrium constant between $A^{\ddagger}$ and A, and Γ is a parameter dominated by tunneling correction. For different isotopologues, the reaction rate constant is different, and the kinetic isotope effect (*KIE*) is defined as (Bigeleisen, 1949; Bigeleisen and Wolfsberg, 1958; Wolfsburg et al., 2010)

$$KIE = \frac{k_H}{k_L} = \frac{K_H^{\ddagger}\Gamma_H}{K_L^{\ddagger}\Gamma_L} \tag{2}$$

where H and L refer to the reaction for isotopologues with heavy and light isotopes, respectively. For elements other than hydrogen, the tunneling effect is negligible (Wolfsburg et al., 2010). Therefore, only $K^{\ddagger}$ is considered for *KIE* calculation in this paper, and $K_H^{\ddagger}/K_L^{\ddagger}$ can be evaluated by the *RPFR* and imaginary frequency ratio which represents the contribution from the decomposition freedom. Then Eq. (2) will become (Bigeleisen and Wolfsberg, 1958)

$$KIE = \frac{K_H^{\ddagger}}{K_L^{\ddagger}} = \frac{s_L^{\ddagger}}{s_H^{\ddagger}} \frac{s_H^A}{s_L^A} \frac{RPFR^{\ddagger}}{RPFR^A} \frac{v_H^{\ddagger}}{v_L^{\ddagger}} \tag{3}$$

in which s is symmetry numbers, $RPFR$ is the reduced partition function ratio, and v is the imaginary frequency. In practice, symmetry numbers does not cause isotope fractionation (Wolfsburg et al., 2010), and $RPFR$ can be calculated by (Bigeleisen and Mayer, 1947)

$$RPFR = \prod_{i}^{l} \frac{u_i^*}{u_i} \frac{exp(-u_i^*/2)}{exp(-u_i/2)} \frac{1-exp(-u_i)}{1-\exp(-u_i^*)} \quad (4)$$

where l is the number vibrational degrees of freedom ($l = 3\,N-5$ for linear molecules, $l = 3\,N-6$ for non-linear molecules, and one less for the transition state, and N is the number of atoms in the molecule), u_i is equal to $hc\omega_i/k_BT$, h is the Planck constant, c is the speed of light, ω_i is the ith normal vibration mode, k_B is Boltzmann constant and T is temperature in Kelvin, the terms with star (*) refer to the isotopologues containing the heavy isotopes.

If the reaction coordinate is coupled with other vibrational modes, there will be no analytical solution for the imaginary frequency. In that case, the Monte Carlo method would not be applicable. Therefore, in this paper we use only two-body vibration for the reaction coordinates. The imaginary frequency can therefore be calculated by (Bigeleisen and Wolfsberg, 1958)

$$\frac{v_H^{\ddagger}}{v_L^{\ddagger}} = \sqrt{\frac{\mu_L}{\mu_H}} \quad (5)$$

where μ is the reduced mass for two atoms or two fragments, and it is calculated by

$$\mu = mM/(m+M) \quad (6)$$

Eq. (5) should be considered as the first order approximation for the complete expression of imaginary frequency. The confines of θ_{KIE} given by this study are therefore the conservative one. The confines will be more dispersed if additional complexities of the imaginary frequency are included.

To adapt to the convention of geochemists, we write KIE in a way so that the normal KIE is less than 1.000, which is the opposite of what Bigeleisen and his colleagues initially defined. To obtain the values of KIE^{18}, we set $m = O + M1$ in Eq. (6), in which m is a fragment which has at least one oxygen atom. O represents an oxygen atom which can be isotopically substituted. $M1$ is the mass of m excluding this oxygen isotope. $M1$ is an independent variable set to range from 0 to 300. M in Eq. (6) is another fragment which is another independent variable set to range from 1 to 300.

We apply a range of 1.1333–1.0000 for both $RPFR^{\ddagger}$ and $RPFR^{R}$ for the $^{18}O/^{16}O$ system. The upper limit 1.1333 is set by CO_2, an oxygen-bearing molecule of practical interest that is one of the strongest bound oxygen species. The corresponding $RPFR^{17}$ is constrained by $(RPFR^{18})^{\kappa}$, with κ ranging from 0.5275 to 0.5305. The fact that we allow both $RPFR$s to vary randomly in the same range without certain degree of coupling or constraining constitutes an important feature of this exercise. Simply put, KIEs as defined in Eq. (3) can be smaller than 1.000 (i.e. normal KIE) or larger than 1.000 (i.e. inverse KIE) depending on bond forming or breaking at transition states (Bigeleisen and Wolfsberg, 1958; Westaway, 2007). Our KIEs cover a much more general case than the "normal KIEs" in which the lighter isotopes react faster than the heavy ones.

3.2. Results and discussion on θ_{KIE}

The results show that for normal KIE, most θ_{KIE} fall in a narrow band, with 84% of the results within a band of 0.02 and 72% within a band of 0.01 of the median value of 0.5262. For the inverse KIE, the median θ_{KIE} value is 0.5310, with 82% of the results within a band of 0.02 and 70% within a band of 0.01. The overall α-θ distribution for normal and inverse KIEs is not symmetrical (Fig. 1).

Thus, for all possible scenarios of elemental KIE, we expect to see a spread of θ values, with the deviation from the canonical value most pronounced when KIE^{18} is close to 1.000. Due to the equal probability of $RPFR$ values ranging from 1.000 to 1.1333 for both the reactant and the TS in our model input, the normal and inverse KIE cases equally populate the $\alpha < 1.000$ and $\alpha > 1.000$ sides respectively. The median θ value is ~0.0049 higher for the inverse KIE cases than for the normal ones. This can be explained by the reduced mass term $(\mu_L/\mu_H)^{1/2}$ in Eq. (5) being always <1.000.

4. θ_{EQ}: MODEL PARAMETERS AND RESULTS

Isotope exchange equilibrium between A and B oxygen-bearing species is reached when two elemental kinetic steps, $A \rightarrow B$ and $B \rightarrow A$, have reached the same rate. In that case,

$$\alpha(A-B) = \frac{KIE(B \rightarrow A)}{KIE(A \rightarrow B)} \quad (7)$$

Since the confines of θ_{KIE} have been examined above (Section 3), the only added exercise in our Monte Carlo calculation is to obtain the ratio of two KIEs that share the same TS. There is no additional constraint imparted by this same TS requirement because of the wide range of $RPFR^{\ddagger}$ values that our model allows the TS to assume. Thus, our Monte Carlo simulation for the confines of θ_{eq} is simply to add a division.

The results show a perfectly symmetrical α-θ pattern for all equilibrium processes (Fig. 1B). The mean θ value 0.5285 equals to the median θ value. And 95% of the results lie within a band of 0.02 and 90% of the results lie within a band of 0.01.

5. EFFECTS OF REACTION PROGRESS, UNBALANCED FLUXES, AND REFERENCE FRAME

There can be many different ways to classify reactions processes. Here we explore three increasingly complex systems: (1) reservoir depletion due to reaction progress; (2) reservoir size being depleted and enriched simultaneously but not necessarily in steady-state; and (3) changing reference frames by looking at isotope fractionation behaviors between any two species that are involved in a reaction.

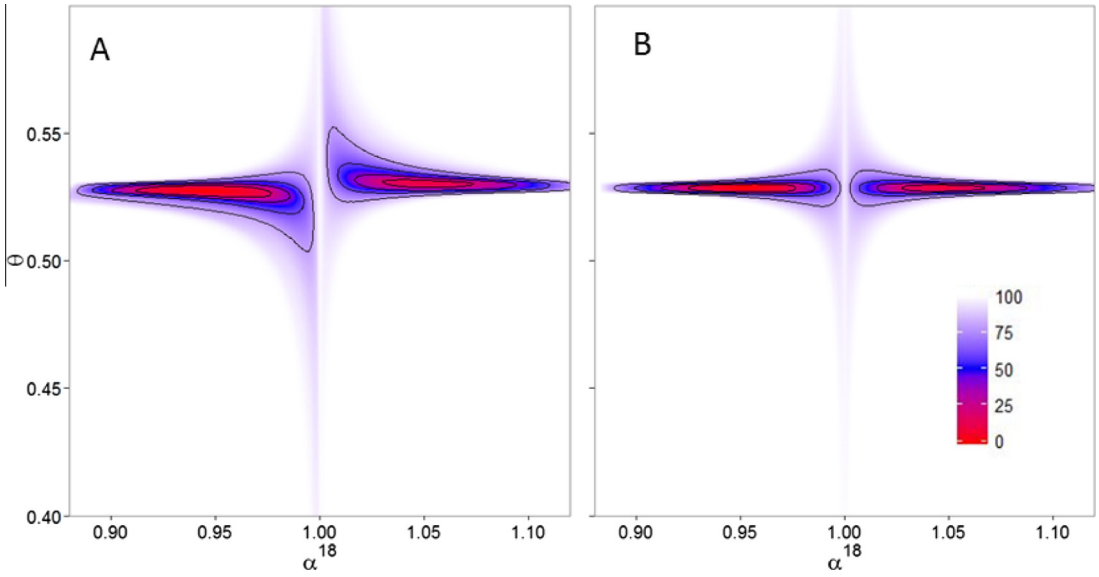

Fig. 1. Plots representing the α-θ distribution of two intrinsic processes: (A) kinetic oxygen isotope fractionation and (B) exchange equilibrium fractionation processes. On panel A, normal *KIE*s cover the left half where KIE^{18} or $\alpha^{18} < 1.000$ while the inverse *KIE* the right half. Contours display regions containing an estimated 25%, 50% and 75% of model results at that density or higher. Colors are a continuous representation of the contours.

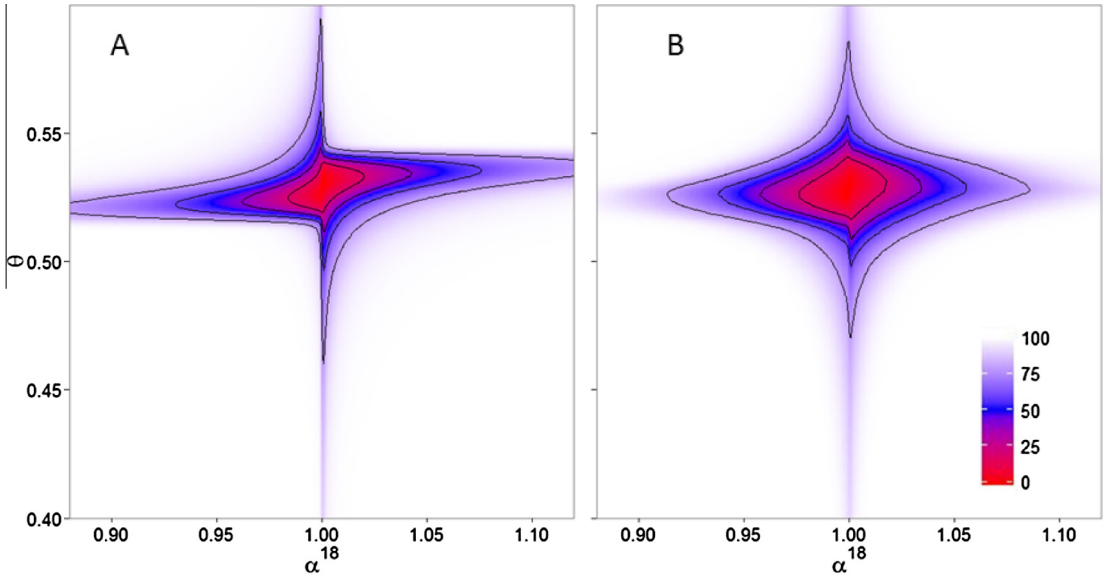

Fig. 2. Plot representing the α-θ distribution of (A) reaction progress when looking at A changing over time and (B) non-steady-state processes between two species or reservoir when looking at A changing over time. Contours display regions containing an estimated 25%, 50% and 75% of model results at that density or higher.

We will examine only the simplest cases where analytical solutions are tenable.

5.1. Reaction progress: Looking at itself changing over time

$$A \rightarrow B$$

$$\frac{R_A}{R_A^0} = \left(\frac{^{16}O}{^{16}O_0}\right)^{KIE-1} \tag{8}$$

when we look at A itself, i.e. the isotope fractionation between R_A (at time t) and R_A^0 (at time $t = 0$), we have

$$\theta = \frac{\ln(^{17}R_A/^{17}R_A^0)}{\ln(^{18}R_A/^{18}R_A^0)} = \frac{^{17}KIE - 1}{^{18}KIE - 1} \tag{9}$$

Here A or B refers to concentration, R the isotope ratio ($^{18}O/^{16}O$ or $^{17}O/^{16}O$), superscript "*" refers to the minor isotopes (^{18}O or ^{17}O), and subscript "0" refers to the corresponding initial values. We use the same parameters we set

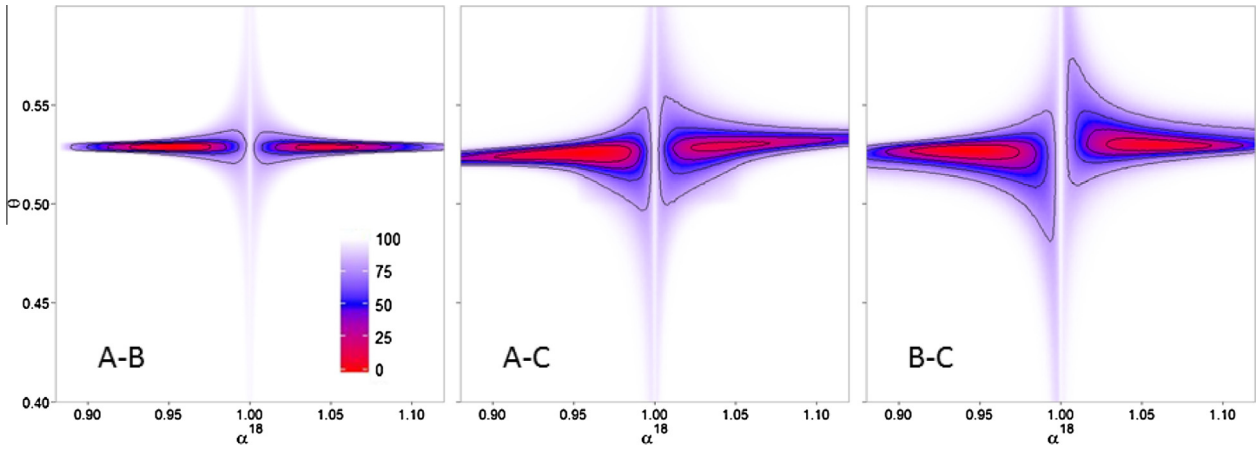

Fig. 3. Plots representing the α-θ distribution of non-equilibrium, three-reservoir reaction systems. Panel A–B, A–C, and B–C represent different reference frames of the same set of reaction systems. Contours display regions containing an estimated 25%, 50% and 75% of model results at that density or higher.

for the θ_{KIE} case (Section 3), and we obtained a distribution that is less symmetrical than that for θ_{eq} (Fig. 2A). Comparing to the case for θ_{eq}, we have here one additional variable $^{16}O/^{16}O_0$ which varies between 1 and 0.

5.2. Non-steady-state between two species or reservoirs

Differing from the *KIE*-level reaction progress case above, this case adds another reaction path that could enrich or deplete the reactant of interest, *A*. This is a case of branching or parallel process. Similarly, we look at *A* evolving over time.

$$A \leftarrow \rightarrow B$$

$$\frac{R_A}{R_A^0}=\frac{1+K_{eq}}{1+K_{eq}\alpha_{eq}}\frac{1+K_0\alpha_0+(K_{eq}\alpha_{eq}-K_0\alpha_0)f^{KIE_b(1+K_{eq}\alpha_{eq})/(1+K_{eq})}}{1+K_0+(K_{eq}-K_0)f} \tag{10}$$

Here $K_{eq}=k_f/k_b=B_{eq}/A_{eq}$, $K_0=B_0/A_0$, $\alpha_{eq}=KIE_f/KIE_b=R_B^{eq}/R_A^{eq}$, $\alpha_0=R_B^0/R_A^0$. *A* or *B* is the concentration, subscript or superscript "0" refers to the respective initial values. Due to the non-equilibrium nature of the systems, additional parameters need to be assigned in order to explore the system's behavior. Compared to the cases for θ_{KIE} and θ_{eq}, additional model parameters include $K_{eq}=0.001$–1000, $K_0=r\times K_{eq}$, $r=0$–2, measuring the deviation of the initial condition from the equilibrium condition, and $f=0$–1, indicating the progress of a reaction toward equilibrium. α_{eq} and θ_{eq} is calculated from forward and backward *KIEs* directly, and forward and backward *KIEs* are calculated as in the case $A\rightarrow B$. We set $\alpha_0=0.96$–1.04 and $\theta_0=0.51$–0.53. These two initial conditions are necessary additional parameters for exploring this non-equilibrium process.

The result displays a distribution pattern more symmetrical and also more dispersed around the origin in the α-θ space (Fig. 2B) than when just looking at the depletion of A over time (Fig. 2A).

5.3. Changing reference frames

The two cases above only looked at a species of interest, *A*, evolving over time. The reference has been *A* itself. However, the θ value can vary with reference frames. Here we examine a simple three-species case as depicted in Eq. (11) to illustrate isotope fractionation behaviors in *A*-*B*, *A*-*C*, and *B*-*C* systems.

$$A \underset{k_{b1}}{\overset{k_{f1}}{\rightleftharpoons}} B \xrightarrow{k_{f2}} C \tag{11}$$

If we assume *B* is at steady state at any instant, then

$$\frac{R_A}{R_A^0}=\left(\frac{A}{A_0}\right)^{\alpha-1} \tag{12}$$

where

$$\alpha=\frac{k_{f1}^*k_{f2}^*}{k_{b1}^*+k_{f2}^*}\frac{k_{b1}+k_{f2}}{k_{f1}k_{f2}} \tag{13}$$

Look at *A*-*B*,

$$\alpha_{AB}=\frac{r_{bf}+KIE_{f2}/KIE_{b1}}{\alpha_{eq1}(r_{bf}+1)} \tag{14}$$

in which $r_{bf}=k_{b1}/k_{f2}$.

Look at *A*-*C*,

$$\frac{R_C}{R_A^0}=\frac{r_{CA}\alpha_0+(1-f^\alpha)}{r_{CA}+1-f} \tag{15}$$

where $r_{CA}=C_0/A_0$, $\alpha_0={R_C}^0/{R_A}^0$, and

$$f=\exp\left(-\frac{k_{f1}k_{f2}}{k_{b1}+k_{f2}}t\right)$$

$$\alpha=\frac{k_{f1}^*k_{f2}^*}{k_{b1}^*+k_{f2}^*}\frac{k_{b1}+k_{f2}}{k_{f1}k_{f2}}=\alpha_{eq1}\frac{KIE_{b1}KIE_{f2}(r_{bf}+1)}{r_{bf}KIE_{b1}+KIE_{f2}}$$

$$\alpha_{AC}=\frac{R_A}{R_C}=\frac{f^{\alpha-1}(r_{CA}+1-f)}{r_{CA}\alpha_0+(1-f^\alpha)} \tag{16}$$

Look at *B*-*C*,

$$\alpha_{BC} = \frac{R_B}{R_C} = \frac{\alpha_{AC}}{\alpha_{AB}} = \frac{f^{\alpha-1}(r_{CA} + 1 - f)}{r_{CA}\alpha_0 + (1 - f^{\alpha})} \frac{\alpha_{eq1}(r_{bf} + 1)}{r_{bf} + KIE_{f2}/KIE_{b1}} \quad (17)$$

As depicted in Fig. 3, although the three cases belong to the same reaction processes, their α-θ spaces are discernibly different due to different reference frames.

5.4. Comparison of α-θ distribution probability among the modeled cases

One way to quantitatively compare the α-θ distributions among the different cases is to compare certain probabilities with those of a reference case. Here we use the equilibrium case as our reference because of its narrowest α-θ distribution. Table 1 illustrates the relative differences in distribution listed according to data-point coverage at 25%, 50%, and 75% levels. In general, the more degrees of freedom a process has the higher probability its θ value will be deviating from the canonical values. A process that has balanced forward and backward fluxes tends to have more confined and more symmetrical α-θ distribution. The non-equilibrium $A \leftrightarrow B$ case and $A \leftrightarrow B \rightarrow C$ case when looked at *B* to *C* exhibit some of the largest spreads in the α-θ space.

5.5. $\Delta\Delta^{17}O$ vs. $\Delta\delta^{18}O$

Our exercise so far has demonstrated that there exists a possibility of non-canonical θ values occurring as the result of the combination of multiple mass-dependent processes. However, an important parameter to evaluate a set of processes is the difference in $\Delta^{17}O$ values or the $\Delta\Delta^{17}O$ between two related species A_0 and A_t or *A* and *B* in a set of processes. When the value of λ is set at the mean θ value of 0.5285 and no intercept is used, it is found that in all equilibrium processes, $\Delta\Delta^{17}O$ is 75% within ±0.10‰ and 90% within ±0.15‰, with maximum and minimum values of 0.36‰ and −0.36‰ respectively, even when the corresponding $\delta^{18}O$ varies from −100‰ to 100‰ (Fig. 4A). This is a much narrower range than that of the corresponding θ values. For the non-equilibrium $A \leftrightarrow B$ case that has one of the largest spreads in θ values, the $\Delta\Delta^{17}O$ is 75% within ±0.3‰, 90% within ±0.50‰, and a more significant range of $\Delta\Delta^{17}O$ at extreme fractionations ($|\Delta\delta^{18}O|$ >100‰) with the value reaching as high as 4.56‰ and below –10‰ (Fig. 4B). These extreme values are, however, rare and $\Delta\Delta^{17}O$ greater than ±1‰ constitutes less than 1% of the model results. We, therefore, recommend that when evaluating if a process or a set of processes has mass-anomalous isotope fractionation we shall look at both the apparent θ and the $\Delta\Delta^{17}O$ between two related species. The $\Delta\Delta^{17}O$ normalizes the influence of the $\Delta\delta'^{18}O$ and alleviates the problem associated with the θ values at α close to 1.000.

6. COMPOUNDED RESERVOIR-TRANSPORT EFFECTS

So far we have explored the confines of intrinsic θ values (θ_{eq} and θ_{KIE}) as well as apparent θ and $\Delta\Delta^{17}O$ values for a set of simple reactions systems where analytical solutions are readily available. We have seen that the apparent θ values can be variable and beyond the canonical confines. Those analytical solutions can provide us some insight into the process in question. It should be pointed out that the analytically derived apparent θ value from intrinsic θ values is largely not applicable to most natural or industrial processes that involve more complex reservoir and transport effects. Determining the $\Delta\Delta^{17}O$ or apparent θ value for complex processes must resort to numerical solutions. Conversely, when an apparent non-canonical θ value is observed for a reaction process, both the intrinsic θs for elemental steps and the associated reservoir-transport effect for that process must be thoroughly examined before the underlying physiochemical nature of the reaction can be concluded. To illustrate this point, we present here two examples – Rayleigh Distillation (RD) and Fractional Distillation (FD) – where the basic step bears a constant set of apparent α and θ values and these values do not change but the reservoir-transport effect changes. In RD process, the apparent θ for all reservoirs at all time equals

Table 1
Relative degrees of confines in the α-θ distribution for different model cases. Areas are calculated by transformation of a 2-D kernel density estimate of the model results.

Model case	Data points covered			Data points	Probability
	25%	50%	75%	omitted (%)	of $\alpha < 1$ (%)
Equilibrium*	1.00	1.00	1.00	0.86	50.0
"Normal" *KIE*	0.73	0.77	0.84	0.44	100.0
All *KIE*	1.46	1.54	1.64	0.88	54.3
Reaction progress (A_0 to A_t)	1.61	2.09	2.72	0.89	45.7
A↔B (A_0 to A_t)	2.58	2.81	3.01	0.86	49.6
A↔B→C					
(A to B)	1.14	1.14	1.14	0.70	50.0
(A to C)	2.85	3.22	3.57	0.89	49.9
(B to C)	3.06	3.48	4.05	0.92	50.2

* The regions with cumulative sums equal to or greater than 25%, 50% and 75% respectively are counted. The resulting numbers are divided by the total number of regions (1,000,000) and the result is adjusted to correspond to the area in terms of the plot axes. These areas are normalized to the equilibrium model results. Values larger than 1.00 cover a larger region of the plot space than the equilibrium model.

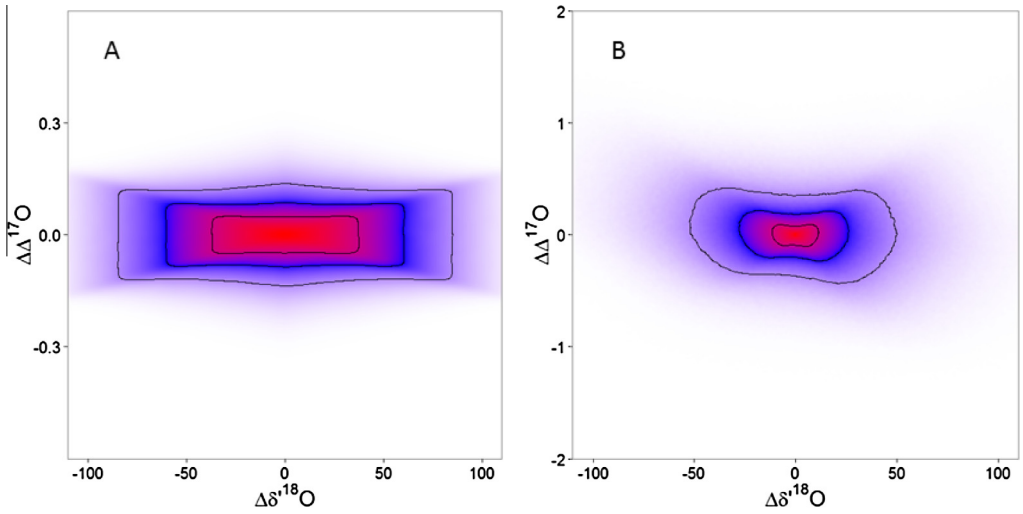

Fig. 4. Plots representing the distribution of $\Delta\delta'^{18}O$ and the change in $\Delta^{17}O$ (i.e. $\Delta\Delta^{17}O$) in equilibrium oxygen isotope exchange processes (A) and for non-equilibrium A↔B processes when looking at A changing over time (B). $\Delta\delta'^{18}O = 1000‰ \ln(\alpha^{18})$. The $\Delta^{17}O$ definition here uses a C of 0.5285 derived from the median θ of the equilibrium model with no intercept. Contours display regions containing an estimated 25%, 50% and 75% of model results at that density or higher. All values are in ‰.

to the apparent θ of the basic step but the $\Delta^{17}O$ of reservoirs deviates gradually and reaches non-canonical values with increasing deviation of the $\delta^{18}O$ value (or $\Delta\delta^{18}O$). In FD process, however, the slope in a $\delta'^{17}O$–$\delta'^{18}O$ space approaches either 1.000 or 0.000 depending on the sign of $ln\alpha$ while the $\Delta^{17}O$ difference increases quickly with increasing $\delta^{18}O$ deviation.

6.1. Rayleigh Distillation (RD)

The RD discussed here differs from the earlier *KIE*-level reaction progress case in that the RD is more general and the α or θ for the elemental step is not *KIE* or θ_{KIE}. The α or θ for the elemental step can be non-equilibrium or apparent as long as they are constant. The stable isotope RD process can be quantified as

$$\frac{R_{t2}}{R_{t1}} = \left(\frac{^{16}O_{t2}}{^{16}O_{t1}}\right)^{(a-1)} \tag{18}$$

Here R is isotope ratio of either $^{18}O/^{16}O$ or $^{17}O/^{16}O$ and ^{16}O the molar number of ^{16}O at time t2 and time t1, respectively. α is the corresponding isotope fractionation factor which is assumed to be constant.

When we look at the relationship between R^{17} and R^{18} or $\delta'^{17}O$ and $\delta'^{18}O$, two corresponding Eq. (18) are rearranged and their ratio gives

$$\frac{\delta'^{17}O_{t2} - \delta'^{17}O_{t1}}{\delta'^{18}O_{t2} - \delta'^{18}O_{t1}} = \frac{(a^{18})^{\theta} - 1}{(a^{18}) - 1} = S \tag{19}$$

Here S is the slope we see in $\delta'^{17}O$–$\delta'^{18}O$ space. It is clear from Eq. (19) that S is fixed at any time with respect to any two residual reservoirs when the elemental α^{17}, α^{18}, and therefore the apparent θ are fixed for the RD process.

Let's look at how the $\Delta^{17}O$ of the residual reservoir of the RD process is going to change. Since

$$\Delta^{17}O_{t1} = \delta^{17}O_{t1} - C \times \delta^{18}O_{t1} \tag{20}$$

$$\Delta^{17}O_{t2} = \delta^{17}O_{t2} - C \times \delta^{18}O_{t2} \tag{21}$$

We get

$$\Delta\Delta^{17}O_{t2-t1} = \left(\frac{(\alpha^{18})^{\theta} - 1}{\alpha^{18} - 1} - C\right)\Delta\delta^{18}O_{t2-t1} \tag{22}$$

Thus, there is a straight-line relationship between change of $\Delta^{17}O$ and change of $\delta^{18}O$ between any residual reservoirs (Fig. 5). Therefore, for a classical RD process, the apparent θ does not change whereas the $\Delta^{17}O$ will scale with the change in $\delta^{18}O$ value, and can deviate from the terrestrial fractionation line (TFL) (Fig. 5). This RD caused $\Delta^{17}O$ deviation was pointed out by Blunier et al. (2002) before.

6.2. Fractional Distillation (FD)

FD differs from RD in that the vapor phase has multiple stages and each is isolated from its condensate, and all condensates are transported back to the original pool for distillation. Assuming all subsequent liquid condensates return to the main evaporating pool in 100% efficiency, we have an overall fractionation factor (Fenske, 1932)

$$\alpha_{n-stages} = \alpha^{n} \tag{23}$$

in which α is the vapor–liquid fractionation factor for each stage, and n is the number of theoretical plates or stages. Thus, we have

$$\frac{R_t}{R_0} = \left(\frac{^{16}O_t}{^{16}O_0}\right)^{(a^n-1)} \tag{24}$$

Here R is isotope ratio of either $^{18}O/^{16}O$ or $^{17}O/^{16}O$ and ^{16}O the molar number of ^{16}O at time t and time 0, respectively. Since we maintain $\alpha^{17} = (\alpha^{18})^{\theta}$ for each distillation step, we have

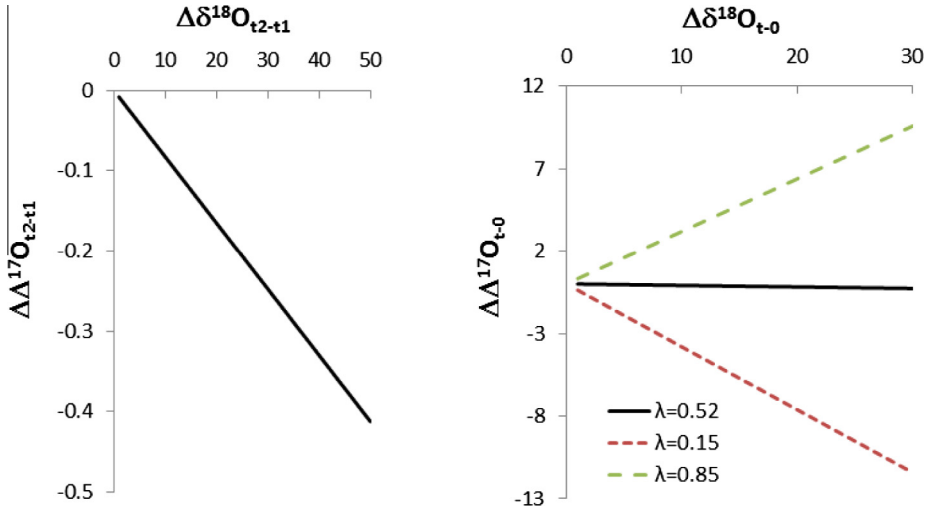

Fig. 5. Changing $\Delta^{17}O$ difference with changing $\delta^{18}O$ of the residues at different times in a classical Rayleigh Distillation process (left panel) or with respect to those of the initial reservoir in a Fractional Distillation process (right panel). Note the vertical scale difference. The black line on the left is a blow-up of the one on the right. Much faster $\Delta\Delta^{17}O$ deviations from zero with increasing $\Delta\delta^{18}O$ are associated with larger deviations of the slope λ from the value of 0.52.

$$\frac{\delta'^{17}O_t - \delta'^{17}O_0}{\delta'^{18}O_t - \delta'^{18}O_0} = \frac{(a^{18})^{\theta n} - 1}{(a^{18})^{n} - 1} = S \tag{25}$$

When the θ, the triple oxygen isotope exponent for each step, is fixed at a canonical value, e.g. 0.520, the triple oxygen isotope slope S in $\delta'^{17}O$–$\delta'^{18}O$ space is therefore a function of α and n. When n approaches a large number (Eq. (25)), the S approaches 1.000 when α is less than 1.000 or S approaches 0.000 when α is larger than 1.000 (Fig. 6). The further the elemental α value deviates from 1.000, the faster the S, or $\Delta\delta^{17}O/\Delta\delta^{18}O$, of a Fractional Distillation process approaches 1.000 or 0.000 (Fig. 6). Here the S and $\Delta^{17}O$ are distinctly beyond their typical mass-dependent values. This is the reason why Fractional Distillation can produce residual water that is enriched mass-anomalously in ^{17}O and ^{18}O with respect to ^{16}O. In other words, even with a fixed canonical θ value, a simple repetition of a process like the FD can yield a non-typical S value and also a large $\Delta^{17}O$ (Fig. 5).

These two simple cases discussed here further strengthens a main point of this study. Due to compounded reservoir-transport effects it is possible to generate non-canonical apparent θ values as well as large $\Delta^{17}O$ even when the θ values for involved elemental steps are canonical. In a process bearing variable canonical θ values in its elemental steps, as demonstrated in this study, the probability of achieving a non-canonical apparent θ might be higher. A slope drawn in the $\delta'^{17}O$–$\delta'^{18}O$ space between data points offers only a superficial clue to the underlying physiochemical nature, and should therefore be interpreted with caution. On the other hand, reservoir-transport effects could have played a role in generating apparent non-mass-dependent isotope signatures in some thermal diffusion or photochemical processes. This is a subject rarely explored at this time, and is certainly beyond the scope of this study.

7. DISCUSSION

It should be pointed out that the intrinsic θ_{KIE} and θ_{eq} values are case specific and are the function of reduced masses, *KIEs*, and temperature. The apparent α and θ of a process, however, vary with additional factors such as initial condition, reaction progress, reservoir, transport, and reference frame, and can be quite different from the intrinsic αs and θs of the many elemental steps involved. Therefore, "a single mass fractionation line" for a set of processes and let alone for the overall Earth materials does not exist in the first place. The observed tight linear correlation between $\delta'^{17}O$ and $\delta'^{18}O$ for most Earth materials, i.e. the TFL, is simply an aggregate of data points from many equilibrium and non-equilibrium processes. The slope of TFL is a statistical result of numerous different yet largely canonical θ_{KIE} and θ_{eq} values on Earth, and is expected to change slightly with the changing population of samples being analyzed. Efforts to do fine calibration on the slope of TFL, therefore, may not contribute to our quest of the underlying mechanisms, i.e. the individual θ, nor does it help with improving the referencing of triple oxygen isotope composition.

Our work differs from Young et al. (2002) in two aspects: (1) we trace the cause to the relationships between the *RPFR*s in the three isotope system; and (2) we use a stochastic approach to evaluate potential combinations of *KIE*s and their different magnitudes and signs of reaction rates. In a parallel effort of evaluating the apparent θ^{33} for multiple sulfur isotope behaviors, Farquhar et al. (2007) examined several models of the sulfate reduction metabolic networks based on known apparent θ values for elemental processes. Again, our treatment is more general.

The results demonstrate that the most compact α-θ space or the narrowest confines of θ are the *A-B* equilibrium cases. In other words, the probability of a non-canonical θ value is less likely for equilibrium processes than for

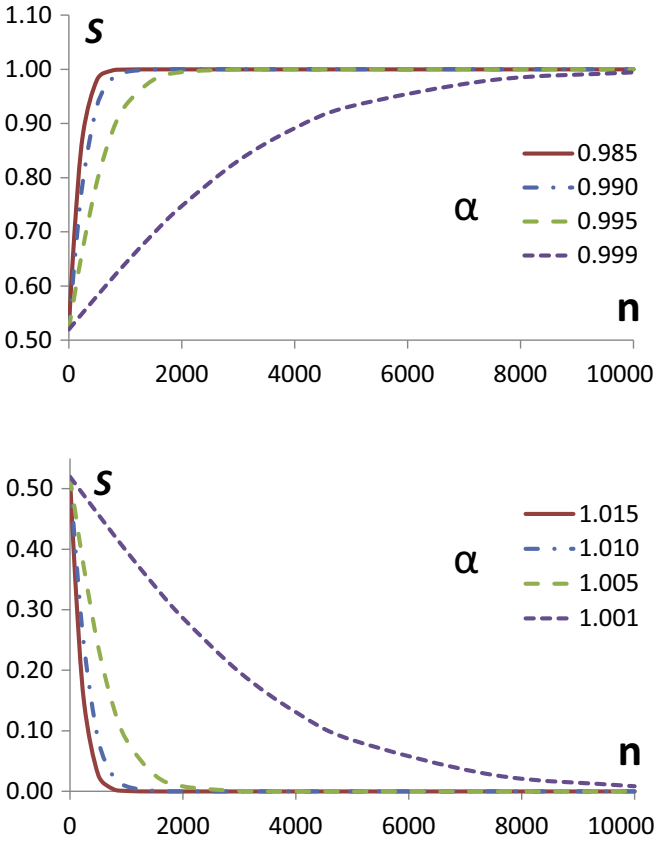

Fig. 6. Changing S values in $\delta'^{17}O$–$\delta'^{18}O$ space at different α and n values in a Fractional Distillation process. α is the fractionation factor for the repeated elemental step, and n is the number of theoretical plates.

non-equilibrium ones. However, although low in probability, the equilibrium cases still have a considerable deviation of the θ value from the canonical one, especially when the α^{18} is close to 1.000. This result echoes earlier statements that at and near "cross-over temperatures", i.e. when $\alpha = 1.000$, anomalous mass effects are expected (Kotaka et al., 1992; Deines, 2003). Deines (2003) attributes the cause of the anomalous mass effect to small differences in the crossover temperature for α^{17} and for α^{18}, which is equivalent to a case when $ln\alpha^{18}$ is at zero whereas the corresponding $ln\alpha^{17}$ at a non-zero value. Viewing from our treatment, it is evident that the root cause is not restricted to a difference in cross-over temperatures. Other variables such as reduced mass, *RPFR*, initial condition, and reaction progress can also result in a θ value being non-canonical. On the other hand, our study also highlights an often omitted fact that when a process is not in equilibrium, its apparent θ value is different from its θ_{eq}. This difference is important because after all we are looking at very small difference in $\Delta^{17}O$.

Eiler et al. (2013) reported a θ value of 0.551 for $ln\alpha^{33}/ln\alpha^{34}$ of sulfur isotope behavior during SF_6 ice-vapor exchange at 137 and 173 K. They interpreted this deviation from an expected canonical value of 0.515 to be the combination of two opposite processes: (1) an inverse sulfur isotope effect between ice and vapor and (2) a normal isotope effect on lattice vibration. Their wide-ranging discussion on potential causes highlights the need to examine the phenomenon. Our study on the probability of a non-canonical θ value rising from a set of strictly mass-dependent processes offers support for their insights. Recent effort in unifying sulfur isotope fractionation behavior during microbial sulfate respiration has also demonstrated the likelihood of the apparent $^{33}\theta$ value deviating from a canonical range (Wing and Halevy, 2014). The challenge is, however, to isolate individual forward and backward *KIE* steps in a composite reaction of interest. So far, few *KIE*s and no θ_{KIE}s of geochemical interests have been determined experimentally or computationally. In light of the wide utilities of and current strong interest in triple isotope relationships, we urge the geochemistry community to take on the challenge.

Finally, reduced masses (μs), *RPFR*s, κ, initial conditions (K_0, α_0, θ_0), reaction progress (f) are among the many randomly varied parameters in our Monte Carlo calculation. Couplings among many of these variables exist and these couplings have not been explored in our exercise. For example, as T increases, κ value approaches 0.5305. That means at high-temperatures the θ will approach 0.5305 and the $\Delta\Delta^{17}O$ to a minimum. In addition, since κ value likely increases with T much faster at lower T than at higher T whereas our Monte Carlo calculation samples

κ value uniformly from 0.5275 to 0.5305, our modeled cases are biased toward lower temperatures (0 to 500 °C). Furthermore, as *RPFR* increases, its κ value will decrease. Large μ values may also correlate with smaller κ values. Therefore, those couplings or secondary relationships can be further examined by this approach.

8. CONCLUSIONS

The triple oxygen isotope composition of an oxygen-bearing compound records its past processes in which two parameters are of intrinsic physical meaning, the θ_{eq} and θ_{KIE}. The challenge has been to deduce these fundamental parameters from observational or experimental data that often involve multiple steps and complex reservoir and transport effects. In this study, we attempt to start from these intrinsic θs, to increase their process complexity, and to examine what the range of the apparent θ can become. We show that a process composed of many mass-dependent elemental steps will, in the highest probability, have a canonical θ value. Distinct deviations are rare but can occur especially when the overall isotope fractionation factor is close to 1.000. The apparent θ value is different from the θ_{eq} when the process is in a non-equilibrium state. Reaction fluxes and θ_{KIE}s are required to determine the apparent θ. Compounded reservoir-transport effects can exert an unexpectedly large role in determining the $\Delta\Delta^{17}O$ value of a process. A slope value in a $\delta'^{17}O$–$\delta'^{18}O$ space can reveal rich information on the underlying reaction pathways and dynamics only if the underlying elemental kinetic steps can be deduced. The community of stable isotope geochemistry is facing an urgent task of calibrating *KIE*s and θ_{KIE}s for important reaction steps involving geochemical H, C, N, O, and S cycles.

ACKNOWLEDGMENTS

H.B. thanks a Visiting Scholar Fund from Institute of Geochemistry, Chinese Academy of Sciences and the Tokyo Institute of Technology Guest Professor program for providing collegial and physical accommodations for his concentration. Financial support is provided by US NSF grant EAR-1251824, China NSFC grant 41490635, and C.L. Jones Professorship to H.B.

APPENDIX A. SUPPLEMENTARY DATA

Supplementary data associated with this article can be found, in the online version, at http://dx.doi.org/10.1016/j.gca.2015.07.038.

REFERENCES

Angert A., Rachmilevitch S., Barkan E. and Luz B. (2003) Effects of photorespiration, the cytochrome pathway, and the alternative pathway on the triple isotopic composition of atmospheric O_2. *Global Biogeochem. Cycles* **17**, 1030.

Angert A., Cappa C. D. and DePaolo D. J. (2004) Kinetic ^{17}O effects in the hydrologic cycle: indirect evidence and implications. *Geochim. Cosmochim. Acta* **68**, 3487–3495.

Bao H., Lyons J. R. and Zhou C. (2008) Triple oxygen isotope evidence for elevated CO_2 levels after a Neoproterozoic glaciation. *Nature* **453**, 504–506.

Barkan E. and Luz B. (2005) High precision measurements of $^{17}O/^{16}O$ and $^{18}O/^{16}O$ ratios in H_2O. *Rapid Commun. Mass Spectrom.* **19**, 3737–3742.

Barkan E. and Luz B. (2007) Diffusivity fractionations of $H_2{}^{16}O/H_2{}^{17}O$ and $H_2{}^{16}O/H_2{}^{18}O$ in air and their implications for isotope hydrology. *Rapid Commun. Mass Spectrom.* **21**, 2999–3005.

Bigeleisen J. (1949) The relative reaction velocities of isotopic molecules. *J. Chem. Phys.* **17**, 675–678.

Bigeleisen J. (1965) Chemistry of isotopes. *Science* **147**, 463–471.

Bigeleisen J. and Mayer M. G. (1947) Calculation of equilibrium constants for isotopic exchange reactions. *J. Chem. Phys.* **15**, 261–267.

Bigeleisen J. and Wolfsberg M. (1953) Fractionation of the carbon isotopes in decarboxylation reactions. 6. Comparison of the intermolecular isotope effects of a pair of isotopic isomers. *J. Chem. Phys.* **21**, 2120–2121.

Bigeleisen J. and Wolfsberg M. (1958) Theoretical and experimental aspects of isotope effects in chemical kinetics. *Adv. Chem. Phys.* **1**, 15–76.

Blunier T., Barnett B., Bender M. L. and Hendricks M. B. (2002) Biological oxygen productivity during the last 60,000 years from triple oxygen isotope measurements. *Global Biogeochem. Cycles* **16**.

Cao X. B. and Liu Y. (2011) Equilibrium mass-dependent fractionation relationships for triple oxygen isotopes. *Geochim. Cosmochim. Acta* **75**, 7435–7445.

Clayton R. N., Grossman L. and Mayeda T. K. (1973) A component of primitive nuclear composition in carbonaceous chondrites. *Science* **182**, 485–488.

Deines P. (2003) A note on intra-elemental isotope effects and the interpretation of non-mass-dependent isotope variations. *Chem. Geol.* **199**, 179–182.

Eiler J., Cartigny P., Hofmann A. E. and Piasecki A. (2013) Non-canonical mass laws in equilibrium isotopic fractionations: evidence from the vapor pressure isotope effect of SF6. *Geochim. Cosmochim. Acta* **107**, 205–219.

Eyring H. (1935) The activated complex in chemical reactions. *J. Chem. Phys.* **3**, 107–115.

Felipe M. A., Xiao Y. T. and Kubicki J. D. (2001) Molecular orbital modeling and transition state theory in geochemistry. In *Molecular Modeling Theory: Applications in the Geosciences* (eds. R. T. Cygan and J. D. Kubicki). Mineralogical Society of America. pp. 485–531.

Fenske M. R. (1932) Fractionation of straight-run Pennsylvania gasoline. *Ind. Eng. Chem.* **24**, 482–485.

Farquhar J., Johnston D. T. and Wing B. A. (2007) Implications of conservation of mass effects on mass-dependent isotope fractionations: influence of network structure on sulfur isotope phase space of dissimilatory sulfate reduction. *Geochim. Cosmochim. Acta* **71**, 5862–5875.

Gehler A., Tutken T. and Pack A. (2011) Triple oxygen isotope analysis of bioapatite as tracer for diagenetic alteration of bones and teeth. *Palaeogeogr. Palaeoclimatol. Palaeoecol.* **310**, 84–91.

Hendricks M. B., Bender M. L., Barnett B. A., Strutton P. and Chavez F. P. (2005) Triple oxygen isotope composition of dissolved O_2 in the equatorial Pacific: a tracer of mixing, production, and respiration. *J. Geophys. Res.-Oceans* **110**.

Herwartz D., Pack A., Friedrichs B. and Bischoff A. (2014) Identification of the giant impactor Theia in lunar rocks. *Science* **344**, 1146–1150.

Herwartz D., Pack A., Krylov D., Xiao Y., Muehlenbachs K., Sengupta S. and Di Rocco T. (2015) Revealing the climate of snowball Earth from $\Delta^{17}O$ systematics of hydrothermal rocks. *Proc. Natl. Acad. Sci.* **112**, 5337–5341.

Hirschi J. and Singleton D. A. (2005) The normal range for secondary Swain-Schaad exponents without tunneling or kinetic complexity. *J. Am. Chem. Soc.* **127**, 3294–3295.

Hoag K. J., Still C. J., Fung I. Y. and Boering K. A. (2005) Triple oxygen isotope composition of tropospheric carbon dioxide as a tracer of terrestrial gross carbon fluxes. *Geophys. Res. Lett.* **32**.

Kotaka M., Okamoto M. and Bigeleisen J. (1992) Anomalous mass effects in isotopic exchange equilibria. *J. Am. Chem. Soc.* **114**, 6436–6445.

Landais A., Barkan E., Yakir D. and Luz B. (2006) The triple isotopic composition of oxygen in leaf water. *Geochim. Cosmochim. Acta* **70**, 4105–4115.

Landais A., Steen-Larsen H. C., Guillevic M., Masson-Delmotte V., Vinther B. and Winkler R. (2012) Triple isotopic composition of oxygen in surface snow and water vapor at NEEM (Greenland). *Geochim. Cosmochim. Acta* **77**, 304–316.

Levin N. E., Raub T. D., Dauphas N. and Eiler J. M. (2014) Triple oxygen isotope variations in sedimentary rocks. *Geochim. Cosmochim. Acta* **139**, 173–189.

Luz B. and Barkan E. (2005) The isotopic ratios $^{17}O/^{16}O$ and $^{18}O/^{16}O$ in molecular oxygen and their significance in biogeochemistry. *Geochim. Cosmochim. Acta* **69**, 1099–1110.

Luz B., Barkan E., Bender M. L., Thiemens M. H. and Boering K. A. (1999) Triple-isotope composition of atmospheric oxygen as a tracer of biosphere productivity. *Nature* **400**, 547–550.

Matsumoto M. and Nishimura T. (1998) Mersenne Twister: a 623-dimensionally equidistributed uniform pseudo-random number generator. *ACM Trans. Model. Comput. Simul.* **8**, 3–30.

Miller M. F. (2002) Isotopic fractionation and the quantification of ^{17}O anomalies in the oxygen three-isotope system: an appraisal and geochemical significance. *Geochim. Cosmochim. Acta* **66**, 1881–1889.

Miller M. F., Franchi I. A., Thiemens M. H., Jackson T. L., Brack A., Kurat G. and Pillinger C. T. (2002) Mass-independent fractionation of oxygen isotopes during thermal decomposition of carbonates. *Proc. Natl. Acad. Sci. U.S.A.* **99**, 10988–10993.

Pack A. and Herwartz D. (2014) The triple oxygen isotope composition of the Earth mantle and understanding $\Delta^{17}O$ variations in terrestrial rocks and minerals. *Earth Planet. Sci. Lett.* **390**, 138–145.

Pack A., Gehler A. and Sussenberger A. (2013) Exploring the usability of isotopically anomalous oxygen in bones and teeth as paleo-CO_2-barometer. *Geochim. Cosmochim. Acta* **102**, 306–317.

Passey et al. (2014) Triple oxygen isotopes in biogenic and sedimentary carbonates. *Geochim. Cosmochim. Acta* **141**, 1–25.

R Development Core Team (2012) R: a language and environment for statistical computing. R Foundation for Statistical Computing.

Rumble D., Miller M. F., Franchi I. A. and Greenwood R. C. (2007) Oxygen three-isotope fractionation lines in terrestrial silicate minerals: an inter-laboratory comparison of hydrothermal quartz and eclogitic garnet. *Geochim. Cosmochim. Acta* **71**, 3592–3600.

Stern M. J. and Vogel P. C. (1971) Relative tritium-deuterium isotope effects in absence of large tunneling factors. *J. Am. Chem. Soc.* **93**, 4664.

Sun T. and Bao H. (2011a) Non-mass-dependent ^{17}O anomalies generated by a superimposed thermal gradient on a rarefied O_2 gas in a closed system. *Rapid Commun. Mass Spectrom.* **25**, 20–24.

Sun T. and Bao H. M. (2011b) Thermal-gradient-induced non-mass-dependent isotope fractionation. *Rapid Commun. Mass Spectrom.* **25**, 765–773.

Thiemens M. H., Chakraborty S. and Jackson T. L. (2014) Decadal $\Delta^{17}O$ record of tropospheric CO_2: verification of a stratospheric component in the troposphere. *J. Geophys. Res.-Atmos.* **119**, 6221–6229.

Wand, M., 2014. KernSmooth: Functions for kernel smoothing for Wand & Jones (1995), R package version 2.23-12 ed.

Westaway K. C. (2007) Determining transition state structure using kinetic isotope effects. *J. Label. Compd. Radiopharm.* **50**, 989–1005.

Wickham H. (2009) *GGPLOT2: Elegant Graphics for Data Analysis*. Springer, New York, pp. 0–0.

Wing B. A. and Halevy I. (2014) Intracellular metabolite levels shape sulfur isotope fractionation during microbial sulfate respiration. *Proc. Natl. Acad. Sci. U.S.A.* **111**, 18116–18125.

Wolfsburg M., Van Hook A. W., Paneth P. and Rebelo L. P. N. (2010) *Isotope Effects: in the Chemical, Geological, and Bio Sciences*. Springer.

Young E. D., Galy A. and Nagahara H. (2002) Kinetic and equilibrium mass-dependent isotope fractionation laws in nature and their geochemical and cosmochemical significance. *Geochim. Cosmochim. Acta* **66**, 1095–1104.

Young E. D., Yeung L. Y. and Kohl I. E. (2014) On the $\Delta^{17}O$ budget of atmospheric O_2. *Geochim. Cosmochim. Acta* **135**, 102–125.

Associate editor: James Farquhar